European Journal of Pharmaceutical Sciences 136 (2019) 104958

Contents lists available at ScienceDirect

European Journal of Pharmaceutical Sciences

journal homepage: www.elsevier.com/locate/ejps

Exploration of long-acting implant formulations of hepatitis B drug entecavir

Steven J. Henry[a], Stephanie E. Barrett[a,*], Seth P. Forster[a], Ryan S. Teller[a], Zhen Yang[a], Li Li[a], Megan A. Mackey[a], Gregory J. Doto[b], Michael P. Ruth[b], Takayuki Tsuchiya[b], Lee J. Klein[a], Marian E. Gindy[a]

[a] Pharmaceutical Sciences, Merck & Co., Inc., 770 Sumneytown Pike, West Point, PA 19486, USA
[b] Safety Assessment and Laboratory Animal Resources (SALAR), Merck & Co., Inc., 770 Sumneytown Pike, West Point, PA 19486, USA

ARTICLE INFO

Keywords:
Entecavir
Hepatitis B
Long-acting parenteral
Subcutaneous implant
Hot melt extrudate

ABSTRACT

Alternative formulations of entecavir, a once daily oral hepatitis B antiretroviral, may improve treatment adherence by patients. We explored the use of biocompatible polymers to control entecavir dissolution in two formats suitable for subcutaneous implantation. Hot melt extrudates were prepared by extruding entecavir-polymer blends at specified weight ratios. Dip-coated tablets were prepared by compressing entecavir in a multi-tip tooling. Tablets were dip-coated in solutions of polymer and dried. In rodents, entecavir-poly(caprolactone) extrudates demonstrated > 180 days of continuous drug release, although below the estimated efficacious target input rate. Drug pharmacokinetic profiles were tunable by varying the polymer employed and implant format. The rank order trends of drug input rates observed *in vitro* were observed *in vivo* in the detected plasma concentrations of entecavir. In all dose groups entecavir was not tolerated locally at the site of administration where adverse event severity correlated with drug input rate. These polymer-based implantable formats have applicability to long-acting formulations of high solubility compounds beyond entecavir.

1. Introduction

Hepatitis B virus infection is considered chronic when levels of viral surface antigen in blood remain elevated for months, failing to elicit concomitant antibody production. Disease progression can be insidious, with chronically infected individuals remaining asymptomatic for decades. Consequently, a third of liver cirrhosis cases and half of hepatocellular carcinoma cases are attributed to chronic hepatitis B induced liver damage (Shepard et al., 2006). Globally, 240–360 million individuals have chronic hepatitis B (Shepard et al., 2006; World Health Organization, 2015). By comparison, 35 million individuals are estimated to be infected with HIV globally (Buell et al., 2015). While pre-exposure vaccination is the most reliable mechanism for halting hepatitis B viral transmission, chronic hepatitis B remains highly endemic (*i.e.* > 8% of the total population) in a number of Asian and African countries. Fortunately, effective nucleos(t)ide reverse transcriptase inhibitors are available for the required lifelong treatment of chronic hepatitis B (Shepard et al., 2006).

Entecavir, a hepatitis B directed nucleoside reverse transcriptase inhibitor, is a first-line antiretroviral agent recommended in the treatment of chronic hepatitis B (World Health Organization, 2015). Entecavir's mechanism of action occurs after viral reverse transcriptase DNA incorporation by impeding elongation (Langley et al., 2007). Presently, entecavir is approved for once daily oral administration (Squibb, 2016). Patient adherence to the treatment regimens of non-curable infectious diseases is critical in preventing disease progression but often hampered by perceived social stigma and the burden of a lifelong drug regimen (Buell et al., 2015).

To reduce this medication adherence burden on chronic hepatitis B patients, we formulated entecavir as hot melt extrudates and encapsulated drug tablets for subcutaneous implantation, targeting six months of drug release. While extended release oral formulations of entecavir have been explored (Venkateswara Reddy et al., 2015), the drug's amenability to long-acting parenteral formulations has received limited attention. Lim and coworkers designed liquid crystal suspensions of entecavir long-acting parenteral administered as subcutaneous injections and successfully demonstrated one to two week drug delivery in rats and beagle dogs (Lim et al., 2015). Ho and coworkers synthesized hydrophobic entecavir pro-drugs by fatty acid conjugation and delivered the pro-drug successfully for four weeks in beagle dogs (Ho

* Corresponding author at: 770 Sumneytown Pike, PO Box 4, WP75B-210, West Point, PA 19486, USA.
E-mail address: stephanie_barrett@merck.com (S.E. Barrett).

https://doi.org/10.1016/j.ejps.2019.104958
Received 5 March 2019; Received in revised form 13 June 2019; Accepted 14 June 2019
Available online 15 June 2019

et al., 2018).

Controlling the high aqueous solubility of entecavir (2.4 mg/mL) (Squibb, 2016) to maintain an efficacious drug input rate from a subcutaneous implant was the principle design challenge. To address this challenge we employed a variety of biocompatible polymers as dissolution controlling matrices in hot melt extrudates and membranes of encapsulated drug tablets. The implantation of hot melt extrudates in the subcutaneous space has precedence in contraception (Funk et al., 2005), treatment of opioid dependence (Braeburn Pharmaceuticals Inc, 2015), and treatment of schizophrenia (Amann et al., 2010). The use of drug tablets in the subcutaneous space has historical roots in the subdermal dosing of morphine pills during the 1830s (Booth, 1996) and testosterone tablets in the 1930s (Deanesly and Parkes, 1938). The later method has evolved in modern times as a treatment for androgen-deficient men by subdermal implantation of pelletized testosterone hot melt extrudates (Kelleher et al., 2004). Pod-intravaginal rings are another modern application of parenteral tablets, though not for subdermal implantation. These intravaginal devices contain one or more polymer coated drug pellets which release small molecules (Baum et al., 2012) or antibodies (Gunawardana et al., 2014) through precise ring orifices.

These results address the feasibility of a novel formulation approach for entecavir to reduce the patient impact of HBV therapy, demonstrate that biodegradable polymer implants can be for high solubility APIs, and illustrate a novel, high drug loading coated tablet formulation approach that may be suitable for other APIs.

2. Material and methods

2.1. Reagents

Entecavir monohydrate was purchased from Proactive Molecular Research (P43–0065). Polymers were poly(D,L-lactide) (PLA) (Evonik Industries, 100 DL 8A), poly(caprolactone) (PCL) (Evonik Industries, 100 CL 7.5E), 75:25 poly(D,L-lactide-*co*-glycolide) (PLGA) (Evonik Industries 7525 DLG 7E), 80:20 poly(D,L-lactide-co-caprolactone) (PLCL) (Evonik Industries, 8020 DLCL 8E) and Tecophilic poly(urethane) (PU) (Lubrizol, HP-60D-20).

2.2. Hot melt extrudates

Entecavir extrudate rods were prepared by tumble blending polymer and drug in the desired weight ratio on a Turbula T2F mixer. If polymer feedstock was purchased pelletized, cryo-milling was performed after liquid nitrogen treatment to reduce particle size using a Kinematica Polymill with a 2 mm screen, at 5000 rpm. The resulting particles were roughly 0.5–2 mm in diameter. Drug-polymer blends were fed using a vibratory feeder into a custom benchtop twin-screw extruder (Supplementary Material, Fig. S6). Screws were 7.5 mm diameter, contained one 90° mixing element, and were run at 50 rpm. Extrusion was performed through a round, 2 mm diameter die at 60 °C for PCL and 100 °C for PLA. The extrudate diameter was manually monitored using calipers and drawn-down in an attempt to maintain constant surface area in the final implants. After cooling at room temperature, extrudates were manually trimmed to achieve the required dose.

2.3. Coated tablets

A blend of 99% *w*/w entecavir monohydrate and 1% w/w magnesium stearate was prepared and granulated by milling through a No. 30 sieve using a glass pestle. Cakes were formed by slugging 2 g batches of the milled formulation in a 25.4 mm diameter tooling at 20 mm/min to a maximum force of 12 kN. The resulting cakes were subsequently milled through a No. 18 sieve using a glass pestle. High aspect ratio tablets were prepared by loading a custom die (7 × 3 mm diameter cylinders) for a complementary multi-tip tooling and compressed at 20 mm/min to a maximum force of 20 kN on an Alliance RT/50 (Minnesota Testing Systems). Final tablets were 93% w/w entecavir, accounting for hydrate factor and purity.

Polymer solutions for dip coating were prepared in 10 mL volumes of tetrahydrofuran (THF) (PU: 0.8 g, PLGA: 1.8 g, and PLCL: 1.6 g) by shaking at 450 rpm overnight at 60 °C. Tablets were suspended from reverse-action forceps (Fig. 2 B and Supplementary Materials Fig. S1) and manually dipped to approximately 75% of their length in the polymer solution. After retraction excess polymer was wicked away by brief contact with a sheet of aluminum foil. The tablet dried for approximately 45 min before reorientation (*i.e.* flipping) and re-dipping. This dip-flip-dip sequence was repeated until the target membrane thickness of 120 μm was achieved. After the final dip, tablets were dried 48 h in a chemical fume hood. Membrane thickness was assayed by calipers and X-ray computed tomography.

2.4. In vitro release assay

Extrudates and tablets were placed in a volume of phosphate buffered saline (PBS) (Hyclone, SH30256.02, Phosphate Buffered Saline (PBS), 1×, 0.0067 M Phosphate, without Calcium, Magnesium) to achieve 3× sink relative to the maximum aqueous solubility of entecavir (~ 2 mg/mL) (Squibb, 2016). Samples were placed in a volume of PBS such that at complete drug dissolution the final concentration of entecavir would be ≤0.67 mg/mL in PBS at 37 °C, *i.e.* 50 mL vials for the extrudates and 250 mL jars for the coated tablets. Release bottles were subjected to continuous shaking at 50 rpm in a 37 °C incubator. Samples were collected at specified time points and an equivalent volume of fresh PBS added back to the release vessel to maintain constant volume.

2.5. Liquid chromatography

At designated time points a 600 μL sample was extracted from each *in vitro* release vessel and an equivalent volume of fresh PBS replaced. Samples were centrifuged at 20,800 x*g* for 5 min. 500 μL supernatant was retained and, if necessary, diluted in PBS before liquid chromatography analysis on an Agilent 1100. Dissolution quantification was performed using a 6 min isocratic method at 40 °C on an Ascentis Express C18 (#53829-U) 15 cm × 4.6 mm, 2.7 μm column. Mobile phase was pumped at 1.5 mL/min and consisted of 98% aqueous (1:99 *v*/v phosphoric acid:water) and 2% organic (50:50 v/v acetonitrile:methanol) components. Injection volume was 6 μL on a 900 μL loop. Degradant detection was performed using a 45 min gradient method at 25 °C on an Atlantis T3 (#186003748) 25 cm × 4.6 mm, 5 μm column. Mobile phase was pumped at 1 mL/min and consisted of aqueous (1:99 v/v trifluoroacetic acid:water) and organic (1:99 v/v trifluoroacetic acid:acetonitrile) components in the time-dependent ratios reported in Table S1. Injection volume was 10 μL on a 900 μL loop. Detection of entecavir was by ultraviolet absorbance at 255 nm for both methods.

2.6. In vivo assay

Four Wistar han rats (two male, two female) per formulation were dosed subcutaneously in a protocol approved the Institutional Review Board of Merck & Co., Inc. Hot melt extrudates were dosed at 100 mg/kg *via* trocar injection. Coated tablets were dosed at 350 mg/kg *via* incision and staple closure. Rats were housed pair-wise, segregated by sex and formulation condition, and monitored for clinical signs. Periodic bleeding was performed to assay entecavir plasma content. If present, implants were recovered at necropsy and stored at −20 °C until characterization. Sections of implantation sites were prepared and examined histomorphologically by an American College of Veterinary Pathologists board-certified veterinary pathologist. All animal

experiments were carried out in accordance with the National Institutes of Health guide for the care and use of Laboratory animals (Approval#: 2016–600,813-APR).

2.7. Numerical deconvolution of pharmacokinetic data

All deconvolution analysis was performed by employing the deconvolution module in Phoenix™ WinNonlin 6.3 software (Pharsight, Certara™ Company). A unit impulse response function was first established using intravenous bolus pharmacokinetic data from rats (Fig. S2). Akaike information criterion was then used to select the appropriate 1-, 2-, or 3- compartmental pharmacokinetic model. Secondary parameters were obtained from the suitable pharmacokinetic model. Next, mean long phermacokinetic profiles were deconvolved using these secondary parameters to yield absorption-time profiles including both input rate and cumulative percent release.

2.8. X-ray computed tomography

Characterization of implants was performed by micro-computed tomography on an XRadia XRM 500. Image reconstruction was performed using XRadia reconstruction software. Visualization was achieved using Fiji (Schindelin et al., n.d.).

3. Results

3.1. Hot melt extrudates: in vitro release

PCL and PLA polymers had satisfactory handling characteristics at extrusion temperatures significantly lower than entecavir's melting point (PCL: 60 °C, PLA: 100 °C, entecavir: 220 °C). entecavir-PLA hot melt extrudates were opaque relative to transparent PLA placebos (Fig. 1 A). Variability in extrudate diameter was the consequence of manually pulling extrudates to the target diameter of 2 mm as monitored periodically with calipers. Manual pulling was required because very small batch sizes were extruded, precluding employment of a belt puller or winding machine. Across the ensemble of implants depicted in Fig. 1 B, surface area variability was only 6% (coefficient of variation, $n = 11$ implants). As entecavir drug load increased above 60%, extrudates became chalky and developed rough surfaces as compared to the smooth-walled placebos and low drug load extrudates.

Increasing entecavir hot melt extrudate drug load increased *in vitro* drug release rate (Fig. 1 B). The variable drug load release experiment was designed by changing the release volume of constant geometry implants to achieve sink conditions while maintaining a constant surface area ($495 \pm 30\ mm^2$, n = 11 implants). Substantially faster release of entecavir from PLA extrudates with drug load equal to and > 40% *w*/w as compared to 30% w/w may be the result of a critical percolation threshold of drug in polymer being achieved above 30% w/w drug load (Amsden et al., 1994). After 100 days of *in vitro* release a largely intact core was present in 30% w/w drug load samples (Fig. 1 ii), while nearly all drug had eluted from samples with drug load of 50% w/w and 60% w/w (Fig. 1 iv, v). entecavir release from PLA implants was faster than PCL implants for equivalent drug load and geometry (Fig. 1 C), while the qualitative form of the input curves (Fig. 1 D) was similar.

3.2. Coated tablets: In Vitro release

Entecavir had remarkable intrinsic compressibility enabling 93% w/w drug load (accounting for purity and salt factor) tablets with no binder required for mechanical integrity. A small amount (1% *w*/w) of magnesium stearate was used as lubricant to facilitate dye ejection after compression. The principle advantage of compressed tablets relative to hot melt extrudates was the substantial reduction in implant size for a given dose (Fig. 2 A, Table S2). Given the high aqueous solubility of entecavir, tablets were encapsulated with rate controlling polymer membranes to slow release of the drug. Reducing water ingress and dissolved drug egress are both strategies for slowing drug release. Rate controlling polymer coats were achieved by THF dissolution of PU, PLGA, and PLCL followed by manual dip-coating (Fig. 2 B and Fig. S1) to a target thickness of 120 μm (Fig. 2 C).

Under the *in vitro* release conditions employed (continuous gentle agitation and 37 °C) uncoated tablets were completely dissolved after two weeks (Fig. 2 D "Bare"). The addition of rate controlling polymer membranes substantially slowed tablet dissolution. This may be the result of reduced water permeation or entecavir diffusion through the encapsulating membrane. Non-erodible PU polymer demonstrated steady *in vitro* input over a period of three months (Fig. 2 E "PU"). Unlike PU, for which entecavir release was purely diffusion based, entecavir release from erodible PLGA and PLCL was both diffusion and degradation based. In both PLGA and PLCL an initial slow release phase transitioned to an accelerated release phase after two months (Fig. 2 E "PLGA" and "PLCL"). This accelerated input rate was concomitant with macroscopic coat deterioration in the release vessel. X-ray computed tomography was used to assay the uniformity of manually applied polymer coats prior to *in vitro* release assay (Fig. 2 F) as well as the integrity of PU coats after six months of *in vitro* release assay (Fig. 2 G). In the latter case, coat flexure was an artifact of sample drying prior to imaging. At the time of *in vitro* termination the PU shell was the same geometry as the original encased tablet.

3.3. Entecavir pharmacokinetics in rat after subcutaneous implantation

Having established a variety of *in vitro* entecavir drug release profiles using hot melt extrudates (Fig. 1 D) and coated tablets (Fig. 2 E) we advanced the same formulations into a subcutaneous rat model. Differential dosing of hot melt extrudates at 100 mg entecavir / kg and coated tablets at 350 mg entecavir / kg was necessitated by trocar volume constraints and the reduced drug load of hot melt extrudates (40% *w*/w drug load entecavir) relative to coated tablets (93% w/w drug load entecavir).

At a course level, the rank order trends of drug input rates observed *in vitro* were also observed *in vivo* in the detected plasma concentrations of entecavir (Fig. 3 A) as well as the calculated drug input rate from the implants (Fig. 3 C). Under both *in vitro* and *in vivo* conditions, bare tablets were the fastest entecavir releasers. As with *in vitro* profiles, PLA and PCL hot melt extrudates *in vivo* exhibited rapid decrease in input rate followed by a more gradual decline. The initial burst of entecavir from hot melt extrudates and uncoated tablets *in vitro* and *in vivo* was attributed to surface drug rapidly dissolving. The delayed release of entecavir from PLGA and PLCL coated tablets *in vitro* was also observed *in vivo*. This delay may be the result of reduced water ingress or reduced entecavir diffusivity through PLGA and PLCL relative to PU. A notable departure from the *in vitro* and *in vivo* trends was the behavior of PU coated tablets which demonstrated constant input *in vitro* but a rapidly decreasing input rate *in vivo*. A summary of relevant PK parameters is reported in Table 1.

All of these results must be considered within the context of the observed tissue response at the implantation site. Chronic entecavir exposure in the subcutaneous space resulted in local cutaneous swelling, scab formation, and necrosis around the implant. The onset of these adverse events correlated with the average entecavir input rate from the implant prior to its first appearance (Fig. 3 D). The fastest releasers, including uncoated and PU coated tablets, exhibited the earliest adverse event onset, while the slowest releasers, including PLCL and PLGA coated tables, exhibited delayed adverse event onset.

Histological preparations revealed a locally extensive necrosis adjacent to the implant and ulceration of overlying epidermis that were further supported by a connective tissue response in the subdermal layers. PU results are shown in Fig. 4 and are representative of the terminal AE observed across dose groups. In a parallel study, rats dosed

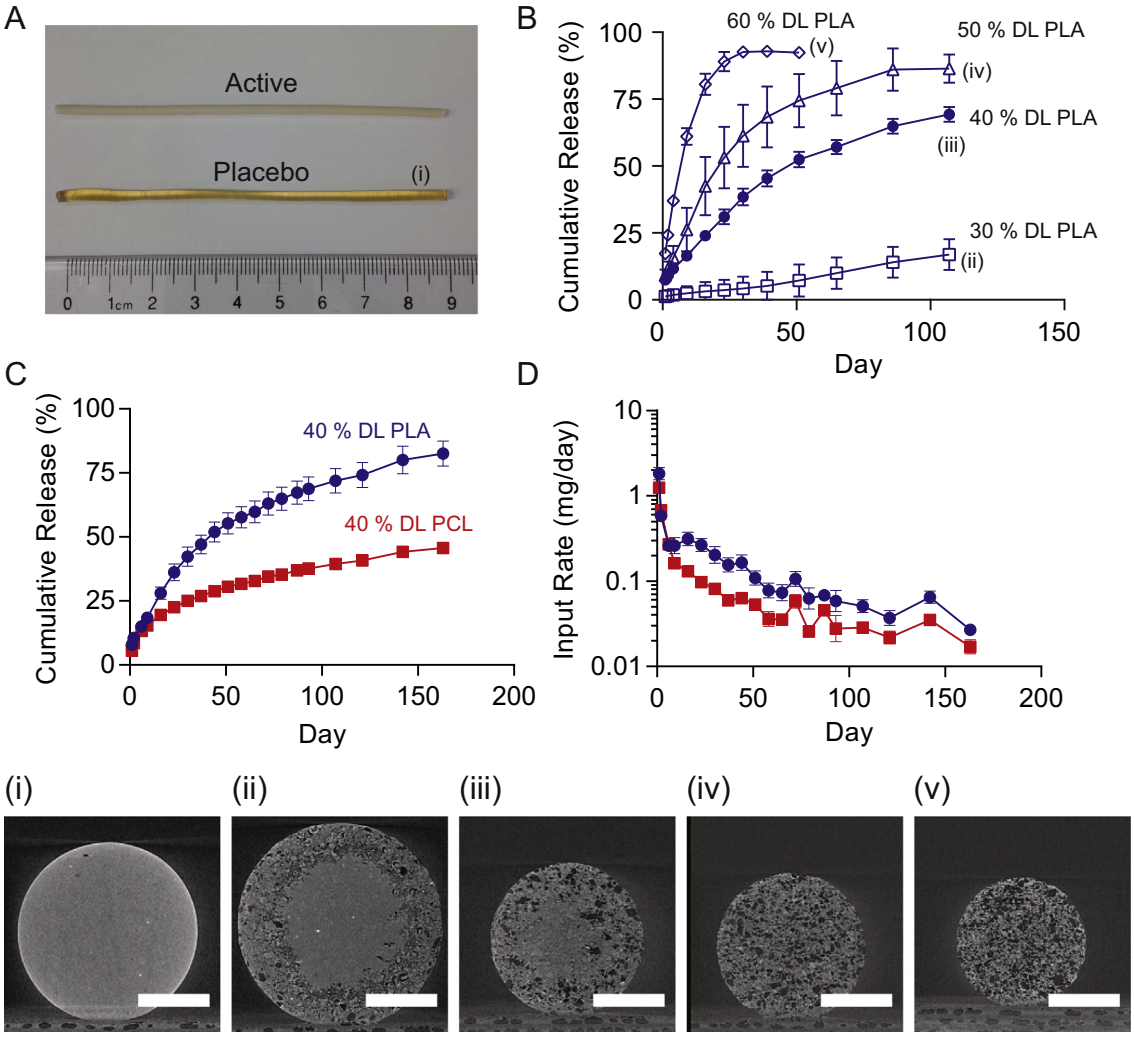

Fig. 1. Hot Melt Extrudate *In Vitro* Release. (A) Placebo and 40% *w*/w drug load PLA hot melt extrudates. (B) Differential release from PLA extrudates as a function of initial drug load. 40% *w*/w drug load PLA and PCL extrudates in terms of (C) cumulative release (D) and instantaneous input rate. X-ray computed tomograms of PLA extrudates: (i) placebo, (ii) 30% w/w drug load at day 107, (iii) 40% w/w drug load at day 107, (iv) 50% w/w drug load at day 107, (v) 60% w/w drug load at day 51 (*in vitro* release experimentation was terminated at day 51 for 60% w/w samples because no further release was observed). Scale bars = 1 mm. Error bars are ± SD (sample counts reported in Table S2 for each condition). "DL" = drug load.

subcutaneously with placebo PLA and PCL extrudates did not exhibit this response. Adverse events were not modality specific, occurring in both hot melt extrudates and tablet dose groups.

With chronic subcutaneous entecavir exposure, progression of the adverse cutaneous response resulted in implant expulsion from the skin. Loss of the implant from the skin was associated with rapid loss of detectable entecavir in the blood plasma. For example, in a rat dosed with an uncoated tablet, recovery of expelled scab tissue on day 80 correlated with the last day of detectable entecavir in the blood plasma at day 87 (Fig. 5 A, green downward triangles). X-ray computed tomography of the recovered scab revealed high contrast flecks, approximately 100 µm long, uniformly distributed throughout (Fig. 5 i). In the future, RAMAN mapping could be performed to assess whether or not these flecks were residual entecavir granules from the original uncoated tablet.

In the recovered PLA implants, a differential erosion pathway was observed with respect to the presence or absence of adhered tissue. An implant recovered cleanly, with no tissue adhesion at day 45 exhibited surface erosion (Fig. 5 ii), while one recovered with tissue adhesion exhibited core erosion (Fig. 5 iii). While different erosion profiles were observed the corresponding pharmcokinetic profiles from these two rats were not markedly different through 45 days (Fig. 5 B). In the recovered PCL implants, at day 185, only core erosion pathways were observed and all three implants exhibited adhered tissue (Fig. 5 iv, v, vi). For the PCL hot melt extrudate dosed rat from which no implant was recovered the corresponding PK curve exhibited a marked decline in plasma entecavir relative to the other three rats from which implants were recovered (Fig. 5 C, gray circles).

Only one PU coated tablet was recovered at necropsy, the remaining implants were presumably expelled in the cage bedding. The adverse connective tissue response and implant expulsion may have contributed to the observed discrepancy between steady input of PU coated tablets *in vitro* and rapidly decreasing input *in vivo*. The observation of tablet surface erosion at the polymer-tablet interface but not at the crack interface (Fig. 5 vii) suggests the tablet was either cracked during extraction or spent very limited time in the subcutaneous space after breaking. The associated pharmacokinetic profile corresponding to the rat with the cracked implant (Fig. 5 D, purple squares) does not have evidence of a crack-associated spike in entecavir plasma concentration. The implication is that dose dumping would not be expected of a broken polymer coated tablet *in vivo* as even uncoated tablets released entecavir in excess of 80 days.

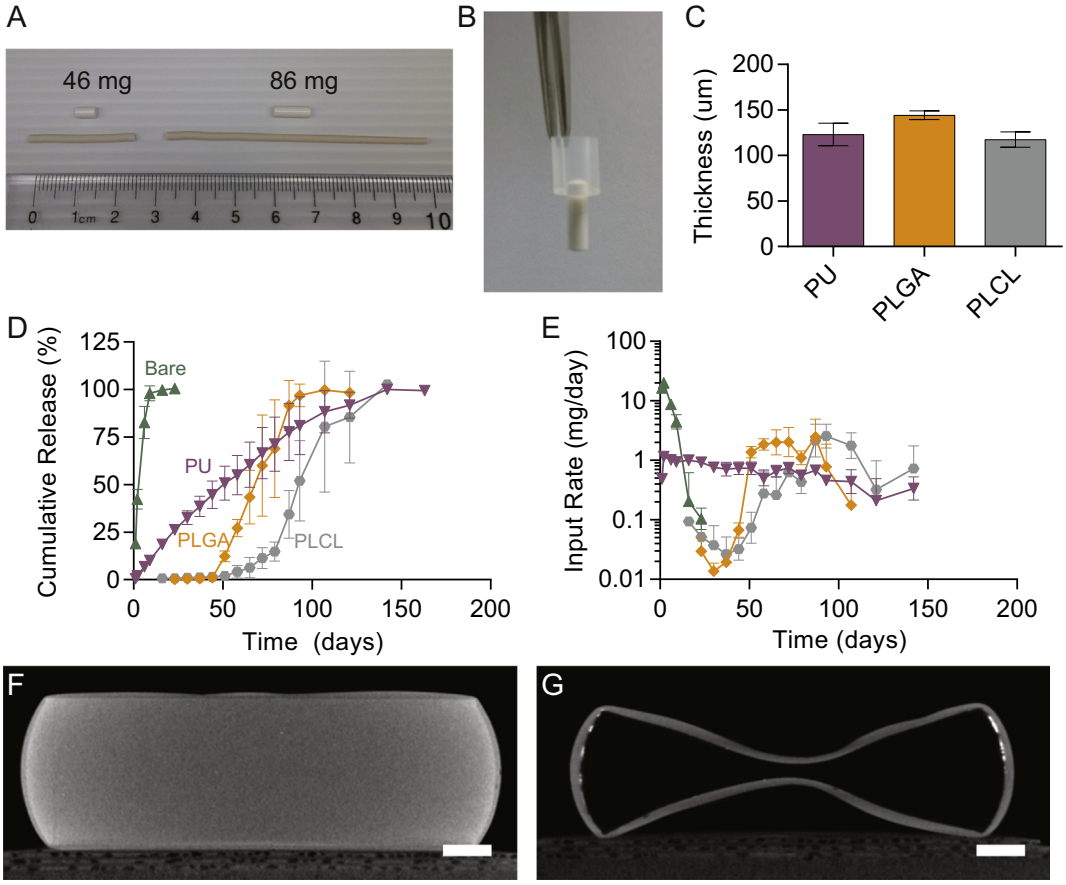

Fig. 2. Coated Tablet *In Vitro* Release. (A) Comparison of equivalent doses for uncoated tablets (93% w/w drug load, top) and HMEs (40% w/w drug load, bottom). (B) Strategy to prevent coat damage during manual dip-flip-dip procedure. (C) Mean coat thickness after manual dip-flip-dip sequence, target thickness was 120 μm. 93% w/w drug load coated tablets in terms of (D) cumulative release and (E) instantaneous input rate. X-ray computed tomograms of PU coated tablet (F) before release and (G) after complete dissolution, day 163. Note: coat flexure was the result of specimen drying. Scale bars = 1 mm. Error bars are ± SD (n = 3 replicates per condition).

4. Discussion

4.1. Hot melt extrudates: in vitro release

PLA and PCL polymers were used as entecavir bioerodible matrices in the preparation of entecavir hot melt extrudates. These polymers were chosen for their differing degradation kinetics, with PLA eroding on the order of half a year *in vivo* (Pitt et al., 1981a) and PCL taking three times longer (Pitt et al., 1981b). However, over the targeted therapeutic duration of six months, entecavir release from the bioerodible polymer matrices was hypothesized to be diffusion based and not by bulk erosion of the polymer.

The chemical basis of PLA's increased drug input rate relative to PCL (Fig. 1 D) remains unclear. Possible explanations include differing drug-polymer miscibility and differing water influx rates as the result of polymer crystallinity. While both polymers are biodegradable (Pitt et al., 1981a; Pitt et al., 1981b), no evidence of an accelerated degradation-based release phase was observed over the six months that implants were assayed *in vitro*. PLA and PCL undergo initial degradation by non-enzymatic random hydrolysis of the polymer backbone. For intrinsic viscosity on the order of 1 dL/g, the initial hydrolytic degradation proceeds approximately three times faster in PLA as compared to PCL (Pitt et al., 1981a). Only after twenty weeks *in vivo* accelerated mass loss begins for PLA (Pitt et al., 1981a), and eighty weeks for PCL (Pitt et al., 1981b). Thus, although PCL is theoretically biodegradable over the lifetime of a patient, it is pragmatically non-erodible over the therapeutic target of six months. Future characterization experiments could include contact angle analysis to access hydrophobicity, water uptake experiments to estimate the volume of water available in diffusion channels, and thin film diffusion experiments to measure drug-in-polymer diffusion coefficients.

4.2. Coated tablets: in vitro release

The two week dissolution of uncoated tablets and the observation of excellent entecavir compressibility suggest tablet hardness could impact dissolution kinetics. While all tablets in this study were produced in an identical manner the hardness was not measured. In the future tablet hardness should be monitored to ensure uniformity.

The selection of nonaqueous THF solvent, which readily dissolved the array of polymers screened in this study, was borne of convenience. For future development, once an appropriate rate-controlling polymer is identified, its solubility in a milder solvent such as acetone would have to be assessed or the complete removal of non-aqueous solvents such as THF assured prior to implantation.

In addition to the PU, PLGA, and PLCL results communicated in Fig. 2, we also assayed for release of entecavir through PCL coated tablets under identical conditions. Ultimately we observed that there was no release in five of six replicates, with the only exception being one replicate in which a coating defect was detected by X-ray computed tomography (Fig. S3 B). The observation of defect-enabled release through PCL suggests doping the coating solution with a small quantity of porogen (*e.g.* salt, sugar, or low molecular weight water-soluble polymers) may be a useful strategy for achieving release-enabling pores

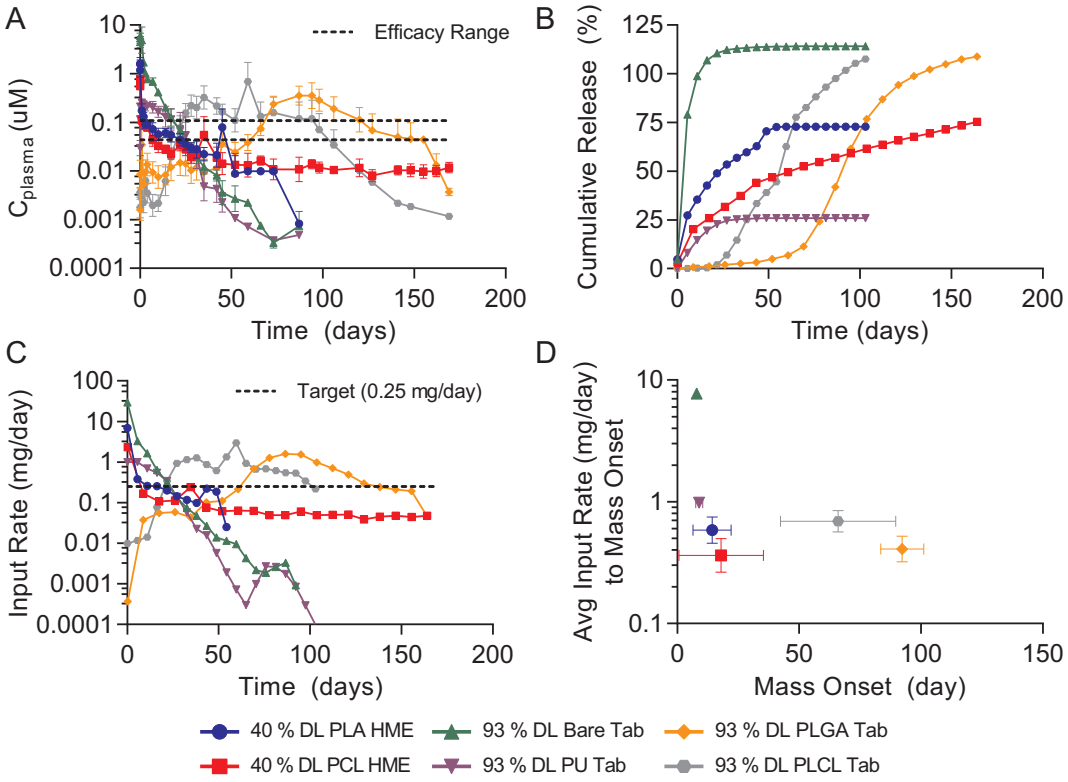

Fig. 3. Rat Pharmacokinetics of Hot Melt Extrudates and Coated Tablets After Subcutaneous Dosing. (A) Mean entecavir plasma concentrations, dotted lines denote estimated rat efficacy. If error bars are absent, only one rat had detectable entecavir at that time point. Calculated (B) cumulative release and (C) input rates, dotted line denotes target input rate. Deconvolution analysis in (B) and (C) was only performed for portions of pharmacokinetic profiles in (A) with at least two rats contributing to the mean plasma concentration. (D) Average entecavir input rate to first observation of adverse cutaneous response at the implant site. Error bars are ± SD. "DL" = drug load, "HME" = hot melt extrudate, "Tab" = tablet.

in the future. The finding that entecavir does not diffuse through competent 120 μm thick PCL coats over six months provides insight into the mechanism of entecavir release from PCL hot melt extrudates. Namely, the lack of entecavir diffusion through PCL membranes implies that the release from entecavir hot melt extrudates is the result of escape through water channels and surface pores. Thus one would anticipate a trapped fraction of entecavir in the core of the PCL hot melt extrudate. Lastly, no crystal form change was detected by X-ray diffraction, performed on hot melt extrudate and tablet formulations before and after fabrication (*i.e.* extrusion or direct compression) (Fig. S4).

4.3. Entecavir pharmacokinetics in rat after subcutaneous implantation

Ultimately, we attribute the tissue response directly to entecavir as it was observed in the uncoated tablet dose group and its onset is directly related to the drug input rate of the implants. The results suggest the polymer systems employed are still amenable to other antiretroviral agents or other therapeutic drug classes.

The PK consequence of circumventing gastrointestinal absorption by subcutaneous delivery of entecavir is unclear and requires further method development to assay liver concentrations of both entecavir and its active triphosphorylated form. Depending on the efficiency of enteral absorption, the actual efficacious dose required for parenteral administration could be lower than the oral dose. Such a reduction is a possibility given that the prescribed oral dose of 0.5 mg/day for non-lamivudine refractory cases is twofold greater than the calculated efficacious input rate of 0.25 mg/day required to achieve steady state blood plasma trough concentrations. This argument and the estimated rat efficacy of 44–109 nM at a 0.25 mg/day input rate are further developed in the Supplementary Material.

Lim and coworkers achieved seven and fourteen day release of entecavir liquid crystal formulations in rats and beagle dogs dosed subcutaneously (Lim et al., 2015). One possibility for the absence of an adverse cutaneous response with liquid crystal formulations of entecavir is that the associated excipients enhanced drug tolerability. Similarly no adverse cutaneous response was observed by Ho and coworkers who dosed beagle dogs subcutaneously with fatty acid conjugated entecavir, measuring parent entecavir in the blood plasma

Table 1
Summary of Pharmacokinetic Metrics. Mean concentration ($< C_{30\text{-last}} >$) and mean input ($< I_{30\text{-last}} >$) were calculated from day 30 to the last time point with at least two rats contributing to the mean. Error bars are ± SD. "HME" = hot melt extrudate. "Tab" = tablet.

	PLA HME	PCL HME	Bare Tab	PU Tab	PLGA Tab	PLCL Tab
T_{max}	90 ± 35 min	90 ± 35 min	9 ± 10 h	3 ± 3 d	82 ± 11 d	55 ± 29 d
C_{max} (μM)	1.7 ± 0.4	0.8 ± 0.1	6.9 ± 2.9	0.3 ± 0.0	0.4 ± 0.3	0.9 ± 0.9
AUC (μM * days)	3 ± 1	3 ± 1	17 ± 5	4 ± 2	16 ± 9	17 ± 9
$< C_{30\text{-last}} >$ (nM)	32 ± 27	15 ± 10	7 ± 7	8 ± 9	176 ± 346	181 ± 174
$< I_{30\text{-last}} >$ (mg/day)	121 ± 92	62 ± 36	17 ± 22	8 ± 16	538 ± 511	896 ± 628
Total release (%)	73	77	114	26	109	108

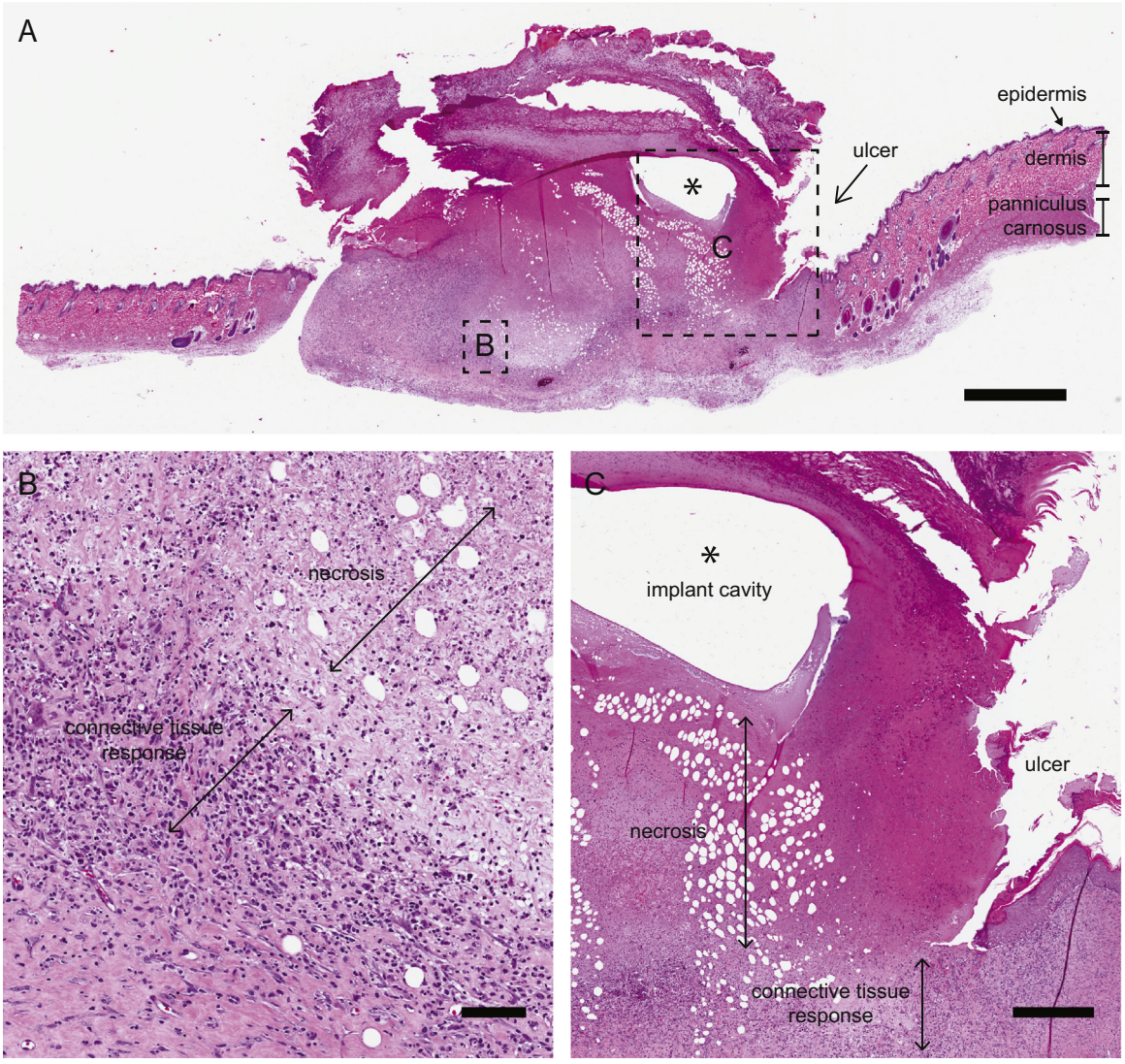

Fig. 4. Histology of tissue around polyurethane (PU) coated tablet. Hematoxylin and Eosin stained sections revealed extensive necrosis around the implant and a connective tissue response in the subdermal layers. The necrotic and connective tissue surrounding the implant elevated the overlying ulcerative epidermis (A to C) causing implant expulsion. Scale bars: (A) 2 mm, (B) 100 µm, and (C) 500 µm. Asterisk denotes implant cavity.

for four weeks (Ho et al., 2018).

The discrepancies could also be attributable to the higher and longer entecavir exposure achieved in our rat studies as compared to those of Lim et al. For example, Lim and coworkers employed a control solution of entecavir dosed at 0.4 mg/kg yielding a C_{max} = 323 ± 45 nM and $AUC_{0\rightarrow last}$ = 23.7 ± 0.6 nM*day, detectable for 12 h. By comparison our control entecavir tablet was dosed at 350 mg/kg yielding a C_{max} = 6.9 ± 2.9 µM and $AUC_{0\rightarrow last}$ = 17.3 ± 4.9 µM*day, detectable for 87 days. Unfortunately, in rats there appears to be no margin of safety between the efficacious doses delivered with subcutaneous implants and the observation of adverse cutaneous responses. Perhaps combination of the implantable systems presented in our work with the liquid crystal (Lim et al., 2015) or fatty acid prodrug approaches (Ho et al., 2018) could achieve longer sustained release as well as avert adverse cutaneous response.

The repeated observation of core erosion correlating with surface tissue adhesion was interesting. One hypothesis is that encapsulation of a biodegradable implant in fibrous connective tissue may create a locally acidic microenvironment that accelerates degradation (Li et al., 1990; Therin et al., 1992). It seems unlikely that the observed core erosion is solely the result of entecavir dissolution as the termini of the implants were also encapsulated in tissue. Fig. S5 illustrates that the thinner the adhered tissue, the closer the voids approach the surface of the implant. Conversely, the thicker the adhered tissue, the farther the voids are from the surface of the implant. While it must be noted that the thickness of the adhered tissue is also a function of the dissector's technique during necropsy, there is a clear relationship between erosion pathway and the presence or absence of tissue adhered to the surface of the implant.

5. Conclusions

In this study, entecavir was not well tolerated at the site of administration at drug input rates estimated to be efficacious for hepatitis B virus treatment. The adverse cutaneous response was attributed directly to the entecavir and not the polymer systems, implying these long-acting implant modalities may still have applicability to other hepatitis B virus non nucleos(t)ide reverse transcriptase inhibitors such as lamivudine, adefovir (Ayoub et al., 2018), and tenofovir. The coated tablet format is particularly attractive for these alternative hepatitis B antiretrovirals which are less potent and require larger doses than entecavir (World Health Organization, 2015).

Ultimately, we demonstrated entecavir release from hot melt extrudates and coated tablets after subcutaneous implantation in rats. A

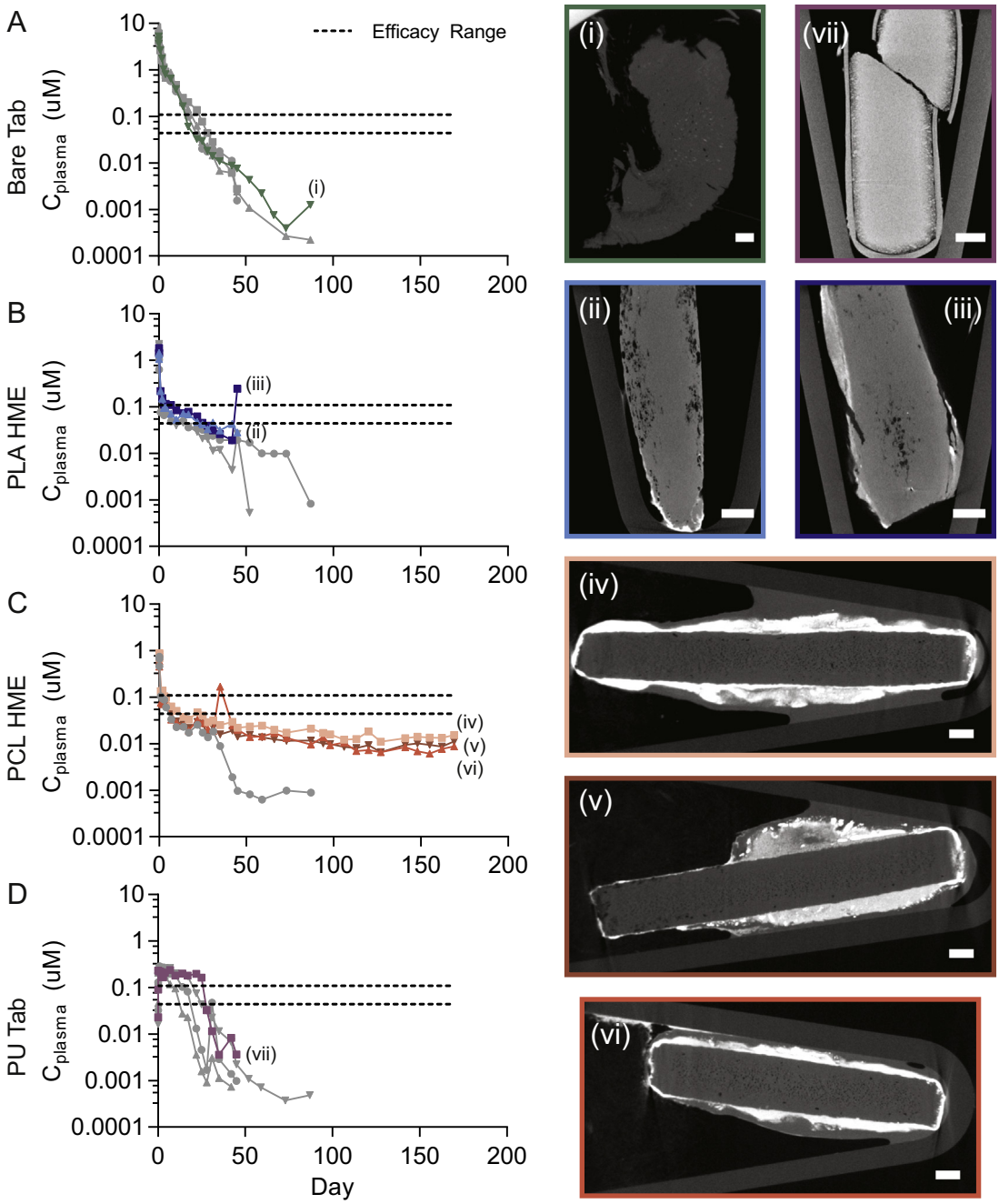

Fig. 5. Individual Rat Pharmacokinetics and X-ray Computed Tomograms of Recovered Implants. Individual rat pharmacokinetic curves for (A) 93 w/w % drug load uncoated tablets, (B) 40% w/w drug load PLA extrudates, (C) 40% w/w drug load PCL extrudates, and (D) 93% drug load PU coated tablets. X-ray computed tomograms: (i) rejected scab recovered on day 80 from the cage of a rat dosed with an uncoated tablet, (ii) PLA extrudate, day 46 without tissue adhesion, (iii) PLA extrudate, day 46 with tissue adhesion, (iv, v, vi) PCL extrudate, day 185 with tissue adhesion, and (vii) PU coated tablet, day 46. Scale bars = 1 mm. Supplementary Fig. S5 repeats panel (v) with enhanced contrast to illustrate differential porosity as a function of adhered tissue thickness. "HME" = hot melt extrudate, "Tab" = tablet.

variety of pharmacokinetic profiles were established by varying the polymer employed as the rate controlling matrix in hot melt extrudates and membranes of encapsulated drug tablets. Both hot melt extrudates and coated tablet implants are amenable to combination therapies which may be necessary in combating drug resistance to monotherapies as a result of patient non-compliance to treatment regimens (Wang, 2013) and may have broader applicability in other therapeutic arenas that require the controlled and sustained release of high solubility compounds.

Declarations of interest

None.

Author statement file

Steven J. Henry: Investigation, Formal Analysis, Writing – Original Draft, Writing – Review & Editing. Stephanie E. Barrett: Conceptualization, Supervision, Writing – Review & Editing, Project Administration. Seth P. Forster: Resources. Ryan S. Teller: Resources. Zhen Yang: Formal Analysis. Li Li: Formal Analysis. Megan A. Mackey:

Resources, Gregory J. Doto: Resources. Michael P. Ruth: Resources. Takayuki Tsuchiya: Resources. Lee J. Klein: Formal Analysis. Marian E. Gindy: Supervision.

Acknowledgements

HPLC troubleshooting by Jeff Smith. X-ray computed tomography assistance by Jerry Klinzing. Bioanalytical support by Elizabeth Mahan, James Marr, and Gary Adamson. Veterinary assistance by Larry Handt. Thoughtful discussions with Steve Ludmerer. Literature and intellectual property searches by Maria Cueto.

Funding

Merck & Co., Inc.

Appendix A. Supplementary data

Supplementary data to this article can be found online at https://doi.org/10.1016/j.ejps.2019.104958.

References

Amann, L.C., Gandal, M.J., Lin, R., Liang, Y., Siegel, S.J., 2010. In vitro-in vivo correlations of scalable PLGA-risperidone implants for the treatment of schizophrenia. Pharm. Res. 27 (8), 1730–1737.

Amsden, B.G., Cheng, Y.-L., Goosen, M.F.A., 1994. A mechanistic study of the release of osmotic agents from polymeric monoliths. J. Control. Release 30 (1), 45–56.

Ayoub, M.M., Elantouny, N.G., El-Nahas, H.M., FE-DS, Ghazy, 2018. Injectable PLGA Adefovir microspheres; the way for long term therapy of chronic hepatitis-B. Eur. J. Pharm. Sci. 118, 24–31.

Baum, M.M., Butkyavichene, I., Gilman, J., Kennedy, S., Kopin, E., Malone, A.M., et al., 2012. An intravaginal ring for the simultaneous delivery of multiple drugs. J. Pharm. Sci. 101 (8), 2833–2843.

Booth, M., 1996. Chapter 5: Heroic Substances. Opium: A History. Simon & Schuster, New York, pp. 67–79.

Braeburn Pharmaceuticals Inc, 2015. PROBUPHINE (buprenorphine HCl) implant CIII treatment of opioid dependence briefing document for the FDA advisory committee meeting December 11, 2015. [16 Feb 2016]; Available from: http://www.fda.gov/downloads/AdvisoryCommittees/CommitteesMeetingMaterials/Drugs/PsychopharmacologicDrugsAdvisoryCommittee/UCM480733.pdf.

Buell, K.G., Chung, C., Chaudhry, Z., Puri, A., Nawab, K., Ravindran, R.P., 2015. Lifelong antiretroviral therapy or HIV cure: the benefits for the individual patient. AIDS Care 1–5.

Deanesly, R., Parkes, A.S., 1938. Further experiments on the administration of hormones by the subcutaneous implantation of tablets. Lancet 232 (6002), 606–609.

Funk, S., Miller, M.M., Mishell Jr., D.R., Archer, D.F., Poindexter, A., Schmidt, J., et al., 2005. Safety and efficacy of Implanon™, a single-rod implantable contraceptive containing etonogestrel. Contraception 71 (5), 319–326.

Gunawardana, M., Baum, M.M., Smith, T.J., Moss, J.A., 2014. An intravaginal ring for the sustained delivery of antibodies. J. Pharm. Sci. 103 (11), 3611–3620.

Ho, M.J., Lee, D.R., Im, S.H., Yoon, J.A., Shin, C.Y., Kim, H.J., et al., 2018. Microsuspension of fatty acid esters of entecavir for parenteral sustained delivery. Int. J. Pharm. 543 (1), 52–59.

Kelleher, S., Howe, C., Conway, A.J., Handelsman, D.J., 2004. Testosterone release rate and duration of action of testosterone pellet implants. Clin. Endocrinol. 60 (4), 420–428.

Langley, D.R., Walsh, A.W., Baldick, C.J., Eggers, B.J., Rose, R.E., Levine, S.M., et al., 2007. Inhibition of hepatitis B virus polymerase by entecavir. J. Virol. 81 (8), 3992–4001.

Li, S.M., Garreau, H., Vert, M., 1990. Structure-property relationships in the case of the degradation of massive aliphatic poly-(α-hydroxy acids) in aqueous media, part 1: poly(DL-lactic acid). J. Mater. Sci. Mater. Med. 1 (3), 123–130.

Lim, J.-L., Ki, M.-H., Joo, M.K., An, S.-W., Hwang, K.-M., Park, E.-S., 2015. An injectable liquid crystal system for sustained delivery of entecavir. Int. J. Pharm. 490 (1–2), 265–272.

Pitt, C.G., Chasalow, F.I., Hibionada, Y.M., Klimas, D.M., Schindler, A., 1981b. Aliphatic polyesters. I. the degradation of poly(ε-caprolactone) in vivo. J. Appl. Polym. Sci. 26 (11), 3779–3787.

Pitt, G.G., Gratzl, M.M., Kimmel, G.L., Surles, J., Sohindler, A., 1981a. Aliphatic polyesters II. The degradation of poly (DL-lactide), poly (ε-caprolactone), and their copolymers in vivo. Biomaterials 2 (4), 215–220.

Schindelin J, Arganda-Carreras I, Frise E, Kaynig V, Longair M, Pietzsch T, et al. Fiji: an open-source platform for biological-image analysis. Nat. Methods.9(7):676–82.

Shepard, C.W., Simard, E.P., Finelli, L., Fiore, A.E., Bell, B.P., 2006. Hepatitis B virus infection: epidemiology and vaccination. Epidemiol. Rev. 28, 112–125.

Bristol-Myers Squibb. BARACLUDE (entecavir) prescribing information. [16 Feb 2016]; Available from: http://www.accessdata.fda.gov/drugsatfda_docs/label/2014/021797s018,021798s019lbl.pdf.

Therin, M., Christel, P., Li, S., Garreau, H., Vert, M., 1992. In vivo degradation of massive poly(α-hydroxy acids): validation of in vitro findings. Biomaterials 13 (9), 594–600.

Venkateswara Reddy, B., Shankar, G., Navaneetha, K., 2015. Design and evaluation of Entecavir sustained release microspheres. Journal of Pharmaceutical and Biomedical Analysis Letters 3 (1), 228–234.

Wang, J., 2013. Clinical utility of entecavir for chronic hepatitis B in Chinese patients. Drug Des Devel Ther 8, 13–24.

World Health Organization, March 2015. Guidelines for the Prevention, Care and Treatment of Persons with Chronic Hepatitis B Infection 2015.